Available online at www.sciencedirect.com
ScienceDirect
Nuclear Instruments and Methods in Physics Research A 586 (2008) 124–128
NUCLEAR INSTRUMENTS & METHODS IN PHYSICS RESEARCH Section A
www.elsevier.com/locate/nima

Microfabricated silicon gratings as neutron-optical components

M. Trinker[a,*], E. Jericha[a], R. Loidl[a,b], H. Rauch[a]

[a]*Atominstitut, Vienna University of Technology, A-1020 Vienna, Austria*
[b]*Institute Laue-Langevin, F-38042 Grenoble, France*

Available online 26 December 2007

Abstract

Microfabricated silicon gratings provide unique test procedures for instruments in neutron scattering and the interpretation of experimental data. Ultra-Small Angle Neutron Scattering (USANS) is currently becoming an effective technique for the analysis of structures in the micrometer range. A series of one-dimensional silicon gratings was fabricated using a highly anisotropic ion etching technique (RIE) and measured at the USANS instrument S18 at ILL, Grenoble. The scattering patterns show up to 17 orders of diffraction, grating parameters derived from these data are in good agreement with the nominal values. Scattering length density correlation functions calculated from the USANS data are compared to Spin Echo SANS (SESANS) correlation functions measured at the Delft University of Technology, demonstrating the complementarity of the two scattering methods.

PACS: 61.12.Ex

Keywords: USANS; Neutron instrumentation; Neutron optics; SESANS

1. Introduction

Ultra-small-angle scattering using perfect silicon crystals was developed decades ago for X-rays [1] and adapted for thermal neutrons [2]. This technique provides a resolution of the order of 10^{-5} Å^{-1} in reciprocal space. The typical structure size probed with the technique ranges from a few tenths of a micrometer up to a few tens of micrometers making this destruction-free method an interesting option for various branches in condensed matter science and technology, e.g. Ref. [3]. Artificial periodic structures have already become a topic of interest for fundamental quantization aspects in neutron optics [4–6]. For the studies presented here a series of silicon gratings with periods ranging from 12 to 28 μm was fabricated using an anisotropic dry etching process (reactive ion etching, RIE) [7,8]. This technique allows for high aspect ratios of the etched features with good profile control. To match the neutron beam cross-section available at the instrument S18 the patterned area of these gratings was chosen exceptionally large at $22 \times 22\,\mathrm{mm}^2$. After optimization of the etching process a nearly ideally rectangular profile of the trenches was achieved [9], Fig. 1.

2. Experimental

Experiments were performed with the USANS option of the instrument S18 at the ILL, Grenoble. The set-up is a double perfect crystal diffractometer in Bonse–Hart configuration with two triple-bounce channel-cut perfect silicon crystals serving as monochromator and analyser, which are mounted on a common optical bench, Fig. 2. The crystals are optimized for Bragg reflections under 30° from the [2 2 0] crystal plane, yielding a neutron wavelength of 1.9 Å after the monochromator. USANS patterns are recorded by rotating the analyser crystal with typical sub-μrad step widths. Exposure times per diffraction pattern range from about 1 to 10 h. The rocking curve $I_R(Q)$ (scattering vector Q in horizontal direction perpendicular to the rotation axis of the analyser and the incoming beam) of the empty instrument is described by a convolution of the reflection curves of the two perfect

*Corresponding author. Tel.: +43 1 58801 54171; fax: +43 1 58801 14199.
E-mail address: mtrinker@ati.ac.at (M. Trinker).

0168-9002/$ - see front matter © 2008 Elsevier B.V. All rights reserved.
doi:10.1016/j.nima.2007.11.042

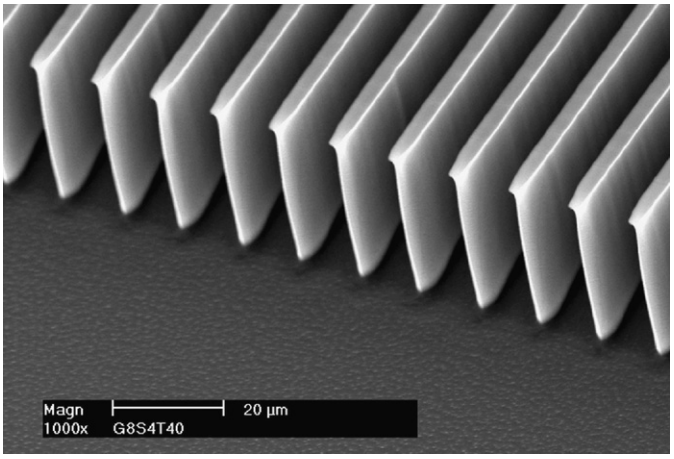

Fig. 1. Grating with period 12 µm, trench depth 40 µm. The optimized etching process creates trenches with excellent control over geometry and depth of the etched features.

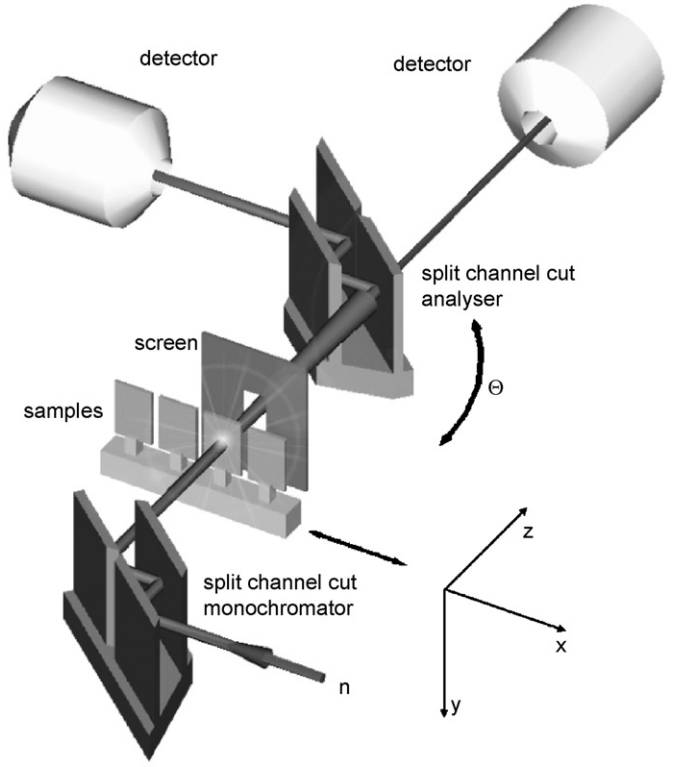

Fig. 2. Scheme of a double crystal diffractometer (Bonse–Hart camera). The scattered intensity is analyzed in the horizontal plane integrating over contributions in vertical direction.

crystals as

$$I_R(Q) = I_0 \int R^3(Q')R^3(Q-Q')\,dQ' + I_B \quad (1)$$

where $R(Q)$ is the reflection probability for a single reflection, I_0 the incoming neutron intensity and I_B the background.

The gratings are placed in the instrument perpendicular to the neutron beam with the trenches in vertical direction. This specific orientation of the line gratings avoids the effect of slit height smearing in the recorded scattering signal. The Bonse–Hart camera resolves the scattered intensity in horizontal direction while the signal is integrated in vertical direction, e.g. Ref. [5].

3. Scattering curves

The density distribution of line gratings does not depend on the coordinate y parallel to the trenches. For small scattering angles the problem can be treated in the plane parallel to the grating surface. This corresponds to the so called projection approximation [10]. The three dimensional scattering length density distribution of the line gratings $\rho(x,y,z)$ is replaced by its projection along the incoming beam.

$$\rho(x) \equiv \int \rho(x,y,z)\,dz = \int \rho(x,z)\,dz \quad (2)$$

where z is the coordinate along the incident neutron beam and (x,y) are the coordinates in the plane of the grating. In Born's approximation the scattering pattern of a periodic structure in the far-field can be decomposed into a form factor $P(Q)$ and a structure factor $S(Q)$

$$I(Q) \propto P(Q)S(Q) \propto |\mathfrak{F}(\rho(x))|^2 \left|\frac{\sin(QNa/2)}{QNa/2}\right|^2 \quad (3)$$

with $\mathfrak{F}(\rho(x))$ the Fourier transform of the one-dimensional scattering length density distribution of the single unit in the grating, and a grating with N scattering units. The function $S(Q)$ exhibits sharp maxima at values

$$Q_n = \frac{2\pi n}{a} \quad (4)$$

where a is the spatial periodicity of the grating. A measurement with a well-resolved diffraction pattern is presented in Fig. 3a. An example for a measurement at the resolution limit of S18 is shown in Fig. 3b. The grating with nominal period 28 µm produces diffraction orders with separation $\Delta Q \approx 2.26 \times 10^{-5}$ Å^{-1} which is close to FWHM of the instrument curve of about 1.9×10^{-5}Å^{-1}. Several conclusions can be drawn from the scattering patterns without further evaluation of the data. The strong variation of the intensities of the diffraction orders and suppression of single peaks in Fig. 3b mean that in this sample high uniformity of the trench profiles across the etched area was achieved. With variations of the profile these phenomena could not occur since contributions from several form factors would lead to a more averaged appearance of the curves. Another result directly obtained from the patterns concerns uniformity of the period in the gratings. A variation of periods would cause broadening of higher orders, which is not observed, see Fig. 3. Evaluation of the scattering patterns yields determination of the grating constants with high precision, Table 1. In cases where the separation of the diffraction orders is higher than the FWHM of the instrument curve, the uncertainty is in

the range of nm. Even for scattering patterns not well resolved by the instrument (gratings with period 28 μm, Fig. 3b) determination of the structure periodicity with a relative precision better than 10^{-3} can be achieved. This is a consequence of the high accessible Q-range and the unrivaled statistics of the instrument S18 and, on the other hand, also reflects the accuracy to which the gratings were fabricated. The observed deviations from the nominal grating periods can be interpreted as about 1% uncertainty in the neutron wavelength λ and instability of the same order over the period in which the measurements were performed.

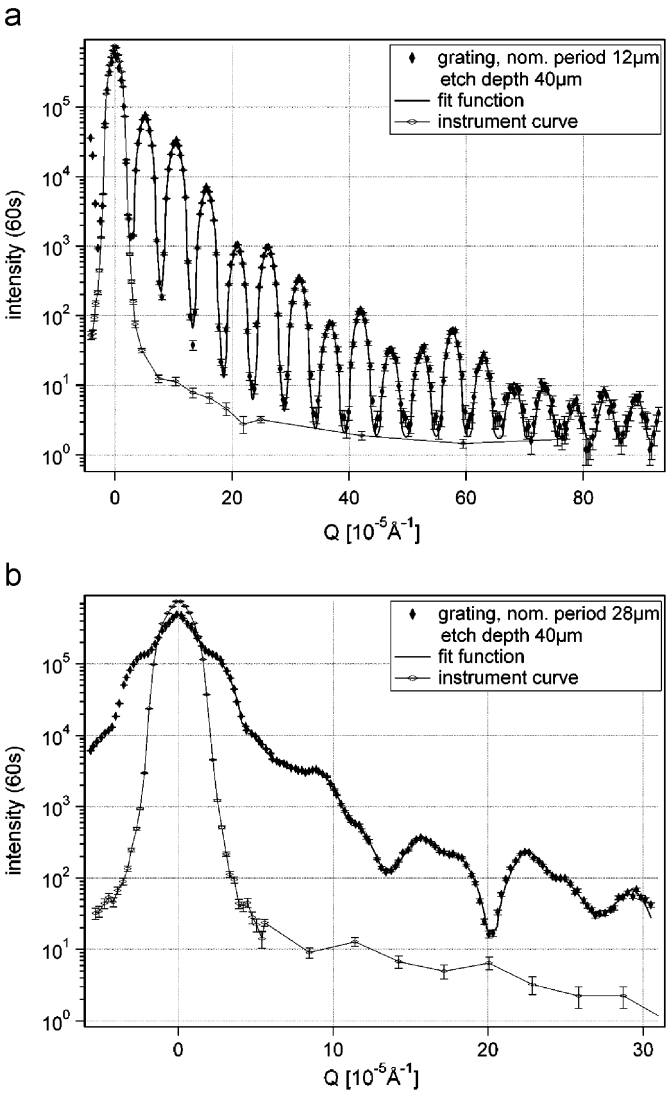

Fig. 3. Scattering patterns obtained from gratings with trench depth 40 μm, periods 12 μm (a), see Fig. 1, and 28 μm (b).

The wavelength of the neutrons in the double crystal diffractometer may be either determined by placing a Fermi-chopper between the monochromator and analyser crystal using time-of-flight over the chopper-detector distance or by rotating the analyser crystal from the non-dispersive orientation into the dispersive position measuring the rotation angle which corresponds to two times the Bragg angle. In both cases we obtain an intensity distribution as a function of the wavelength.

USANS curves are usually measured as function of the analyser rotation angle θ, and the Q-values are obtained by an appropriate scaling of the θ-axis, $Q = 2\pi\theta/\lambda$, where λ is the central wavelength of the distribution. The experimental curves shown in Fig. 3 were obtained in exactly that way. The high uniformity of the line gratings and the precision in their fabrication and in measuring their scattering patterns open another possibility to determine the wavelength needed for the conversion to Q. The periodicity of the lattice may be determined by another method, e.g. by light optics. From this information the position of the diffraction peaks is calculated with Eq. (4) and related to the angular distance $\Delta\theta = \theta_{n+1} - \theta_n$ of the peaks by

$$\lambda = \frac{2\pi\Delta\theta}{\Delta Q} = 2\pi\frac{\theta_{n+1} - \theta_n}{Q_{n+1} - Q_n}. \quad (5)$$

This procedure automatically yields an effective wavelength averaged over the actual wavelength distribution inside the double crystal diffractometer at the sample position of the instrument. Since the measurement of the diffraction pattern of a line grating is straight-forward and does not require a change in the set-up we propose to introduce line gratings as standard neutron-optical components for wavelength determination in a USANS facility. From the values compiled in Table 1 we expect a wavelength accuracy of a few times 10^{-4} by this method.

4. Correlation functions

The scattered intensity $I(Q)$ can be interpreted as the Fourier transform $\mathfrak{F}$ of the Patterson- or autocorrelation

Table 1
Nominal values and experimentally determined periods of various silicon line gratings

Meas. orders	Depth (μm)	ΔQ_{exp} (10^{-5} Å^{-1})	Period (μm) nom.	Period (μm) exp.
17	40	5.2489 ± 0.0007	12	11.970 ± 0.002
12	60	5.2411 ± 0.0009	12	11.988 ± 0.002
13	40	2.2593 ± 0.0009	28	27.810 ± 0.011
12	60	2.2714 ± 0.0014	28	27.662 ± 0.017
12	80	2.2626 ± 0.0012	28	27.770 ± 0.015

function $\gamma(x)$

$$\gamma(x) = \mathfrak{F}^{-1}(I(Q)) = \mathfrak{F}^{-1}(|A(Q)|^2) = \rho(x) \otimes \rho(-x) = \int \rho(u)\rho(u+x)\,\mathrm{d}u \quad (6)$$

where $\rho(x)$ is the scattering length density distribution. Scattering intensity and correlation function form a Fourier pair like scattering amplitude $A(Q)$ and scattering length density distribution $\rho(x)$. For the case of discrete diffraction orders from gratings with period a the Fourier transform can be replaced by a sum. With the symmetry of the problem $\rho(-x) = \rho(x)$ and M measured orders of diffraction one can write for the experimentally accessible quantity $\gamma_{\mathrm{exp}}(x)$

$$\gamma_{\mathrm{exp}}(x) = \sum_{n=1}^{M} C_n \cos\left(\frac{2\pi n x}{a}\right). \quad (7)$$

The coefficients C_n are the intensities of the corresponding diffraction orders. From $\gamma_{\mathrm{exp}}(x)$ normalized correlation functions can be calculated.

In Fig. 4 normalized correlation functions for two gratings with period 12 μm and etch depths of 40 and 60 μm are compared to the correlation function of a rectangular profile. In both cases deviations from the nominal profile are evident. It is known from the development of the etching process that certain variations in the etch profile can occur due to the sensitivity of the process. Underetching of the mask material and premature erosion of the etch mask can cause varying ridge to trench ratios for different samples with identical nominal structure. Furthermore, etch profiles are expected to depend on etch depth. To test for this effect, two gratings with different depth and identical period were measured.

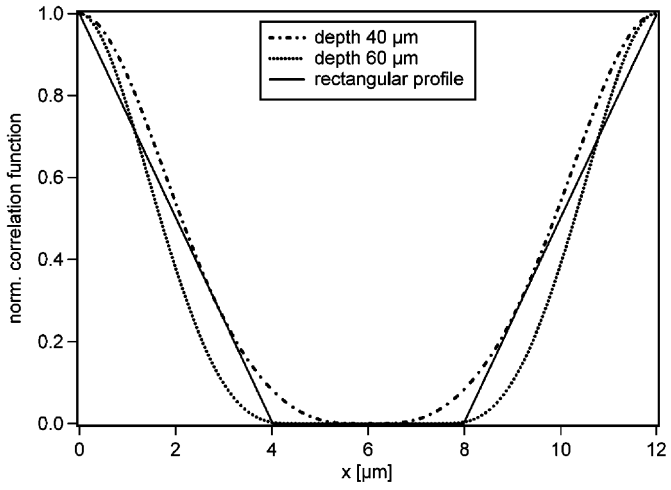

Fig. 4. Correlation functions calculated from USANS data for two gratings with period 12 μm. For both samples with etch depths of 40 μm (dots) and 60 μm (dash-dots) deviations from the nominal rectangular profile (solid line) are evident.

5. Comparison with results from SESANS

The new spin echo SANS technique (SESANS) developed at the Delft University of Technology during recent years measures a signal closely related to the correlation function of the scattering length density distribution [11,12]. The method is based on the Larmor precession of polarized neutrons passing through magnetic fields with inclined faces, Fig. 5. The trajectory of the neutron scattered by the sample is encoded by the precession angle. The measured quantity is the degree of polarization as a function of the spin-echo length x. The degree of polarization is closely related to the SESANS-correlation function $G(x)$:

$$\frac{P(x)}{P_0} = 1 - \sigma t + \sigma t G(x) \quad (8)$$

$$x = \frac{c\lambda^2 BL\cot\theta_0}{2\pi} \quad (9)$$

with σ the total scattering cross-section, and t the thickness of the sample. The spin-echo length depends on the constant $c = 4.6368 \times 10^{14}\,\mathrm{T^{-1}\,m^{-2}}$, the neutron wavelength λ, the magnetic field B, the length L of the precession region and the angle between the incoming neutron beam and the face of the magnetic field regions θ_0. The spin-echo length can be identified with the coordinate x in the sample perpendicular to the incident beam. The function $G(x)$ is the projection of the autocorrelation function of the sample along the direction of the incident beam. Different from conventional SANS and also USANS the measured quantity contains information in real space. For a detailed description of the method see Ref. [12] and references therein.

The two gratings with period 12 μm and etch depths of 40 and 60 μm were measured at the Delft University of Technology. With the sample perpendicular to the incoming beam and the trenches perpendicular to the sensitive direction x the measured signal $G(x)$ corresponds to the autocorrelation function of the scattering length density of the grating perpendicular to the trenches, which is the quantity calculated from the USANS data in the previous section. Uncertainties in the spin-echo length are mainly due to the fact that the effective angle θ_0 is known only up to about 5% [13]. Also the spin-echo length can be calibrated with the periodic silicon structures. For the data presented here calibration resulted in a correction of about 4% of the calculated length scale, Eq. (9). In Fig. 6a,b the experimental data from SESANS are compared to the

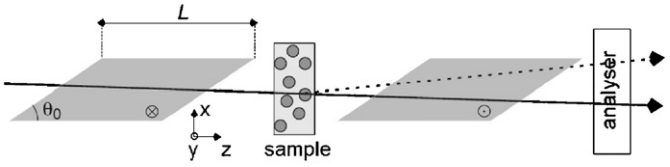

Fig. 5. Scheme of a SESANS setup [12].

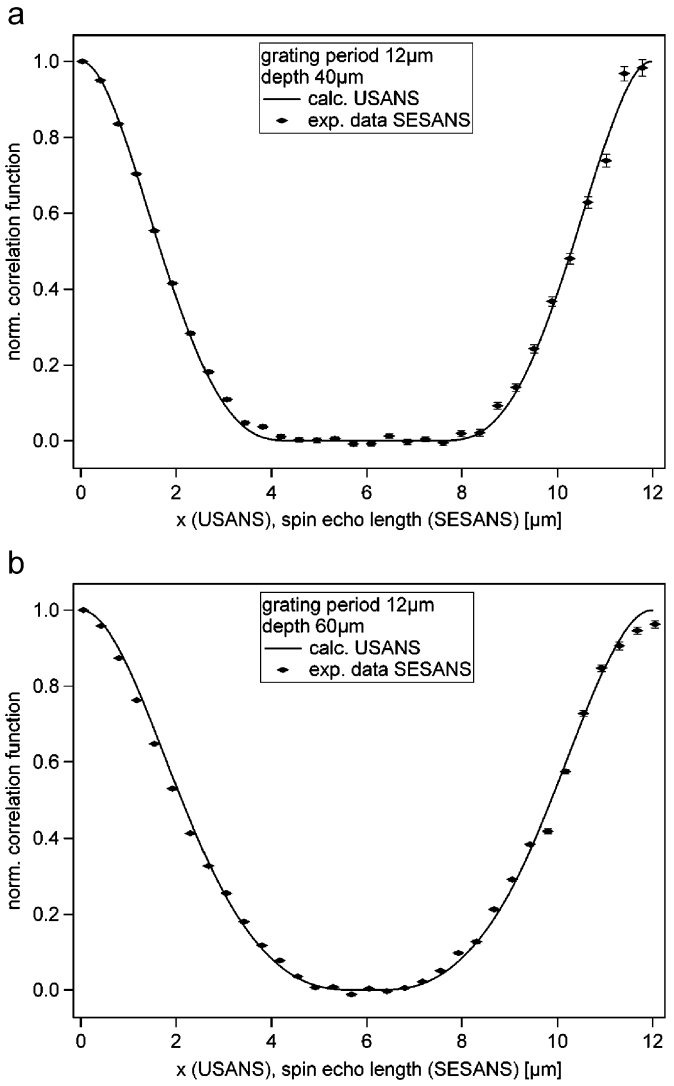

Fig. 6. Experimental data from SESANS and correlation functions calculated from USANS data for two gratings with etching depths 40 µm (a), Fig. 1, and 60 µm (b). The spin-echo length was calibrated with the grating period. Results from the two techniques show excellent agreement.

calculated correlation functions from USANS. The results of the two techniques are found to be in excellent agreement, giving a striking demonstration of the complementarity of the two methods.

6. Summary

We have presented scattering experiments performed on artificial silicon lattices. The model samples developed for these measurements allow a calibration and stability check of neutron small-angle scattering instruments over a wide Q-range. Testing devices and methods with model structures of well-known geometries will further pave the way of ultra-small-angle neutron scattering towards a standard method. The complementarity of USANS and the new SESANS method could be demonstrated by comparison of experimental results from both techniques.

Acknowledgments

We acknowledge K. Unterrainer, G. Strasser and W. Schrenk, Center for Micro- and Nanostructures, Vienna University of Technology, for their support in the development and fabrication of the silicon gratings. We thank M.T. Rekveldt and W.G. Bouwman, Delft University of Technology, for the SESANS data. This work was financially supported by the Austrian Science Fund (FWF), Project FWF-SFB15 No. F1514.

References

[1] U. Bonse, M. Hart, Appl. Phys. Lett. 7 (1965) 238.
[2] D. Schwahn, A. Miksovsky, H. Rauch, E. Seidl, G. Zugarek, Nucl. Instr. and Meth. A 239 (1985) 229.
[3] D.W. Schaefer, M. Agamalin, Curr. Opin. Solid State Mater. Res. 8 (2004) 39.
[4] H. Kurz, H. Rauch, Z. f. Physik 220 (1969) 419.
[5] E. Jericha, M. Baron, M. Hainbuchner, R. Loidl, M. Villa, H. Rauch, J. Appl. Cryst. 36 (2003) 778.
[6] H. Rauch, H. Lemmel, M. Baron, R. Loidl, Nature 417 (2002) 630.
[7] C. Cardinaud, M.-C. Peignon, P.-Y. Tessier, Appl. Surf. Sci. 164 (2000) 72.
[8] M.J. Walker, Proceedings SPIE The International Society for Optical Engineering, vol. 4407, 2001, p. 88.
[9] M. Trinker, Annual Report of The Austrian Society for Micro- and Nanoelectronics (2003) 125.
[10] D.M. Paganin, Coherent X-Ray Optics, Oxford University Press, Oxford, 2006, p. 71.
[11] M.T. Rekveldt, Nucl. Instr. and Meth. B 114 (1996) 366.
[12] W.G. Bouwman, T.V. Kruglov, J. Plomp, M.T. Rekveldt, Physica B 357 (2005) 66.
[13] W.G. Bouwman, private communication.